scientific reports

OPEN

An All-Metal Broadband Low SLL slot array antenna for use in 5G Sub-6 GHz networks

Davood Zarifi[1,3]✉, Ali Farahbakhsh[2,3] & Michal Mrozowski[3]

This paper describes the design and implementation of an all-metal wideband cavity-backed slot array antenna specifically optimized for 5G sub-6 GHz networks. The antenna is engineered to feature low sidelobe levels (SLL), which enhance signal clarity and reduce interference. The proposed antenna utilizes a novel approach, directly exciting all radiating slots through the cavity layer, thus eliminating the need for a complex and lossy power dividing network. The antenna's performance is validated through full-wave simulations and measurements. The results demonstrate antenna's ability to achieve wideband operation from 3.1 to 4 GHz with – 19 dB SLL, peak gain of 20.2 dBi, and more than 90% total efficiency. The main advantages provided by the proposed slot arrays are wide bandwidth, high radiation efficiency, high gain, low sidelobe levels. The all-metal construction ensures robust power handling, and the simplified design contributes to its low complexity. These characteristics make the antenna a promising candidate for 5G deployments.

Fifth-generation (5G) technology represents a fundamental advancement in wireless communication, delivering enhanced performance through increased speeds, reduced latency, and expanded network capacity compared to its predecessors[1]. A key aspect of 5G is its use of various frequency bands, including the sub-6 GHz band (FR1). Sub-6 GHz 5G can support a higher density of connected devices, making them perfect for smart cities, connected homes, and industrial Internet of Things (IoT) applications. The n78 band is a crucial frequency band for 5G sub-6 GHz networks, operating between 3,300 and 3,800 MHz. Often referred to as the 3.5 GHz band or C-band, it is known for its balance of coverage and capacity. The n78 band employs time-division duplexing, allowing the same frequency to be used for uplink and downlink at different times. This method enhances spectrum efficiency and boosts overall network performance. In addition, the Citizens Broadband Radio Service (CBRS) is a 150 MHz spectrum band within the 3.5 GHz range (3,550 MHz to 3,700 MHz). This service (i.e., BRS) is essential for applications such as mobile network densification, fixed wireless access, and the creation of private networks.

Low sidelobe level (SLL) antennas are needed in 5G sub-6 GHz networks for reducing interference and enhancing signal quality[2]. These antennas minimize the power radiated in unwanted directions, thereby boosting the overall performance of the communication system. Low SLL antennas ensure clearer and more reliable connections by suppressing sidelobes, which is particularly important for the dense deployment of 5G networks. Two common techniques for achieving antenna arrays with low SLL are amplitude tapering and employing slant-polarized antenna[3]. Designing low SLL antenna arrays involves non-uniform amplitude distributions such as binomial, Chebyshev, and Taylor distributions. The non-uniform amplitudes of these antenna elements are typically achieved using unequal-power dividing networks. However, these low-sidelobe antennas often have complex structures due to using power dividers. The second technique shifts the antenna's polarization to the diagonal plane of a uniformly excited square array, effectively suppressing SLL[4–7]. The main drawback of these antennas is their multi-layered and complex structure, especially for large arrays.

Over the years, a large variety of printed low SLL antennas were implemented using various printed circuit board (PCB)-based technologies, including microstrip[8–15] and substrate-integrated waveguide (SIW)[16–21]. These antennas provide benefits such as a low profile, cost-efficiency, and versatility in manufacturing and integration. However, they are limited by low power handling capacity and high insertion loss. Conversely, hollow waveguide (HW) antennas, while larger and more expensive, provide high gain, superior efficiency, and robust power handling, making them well-suited for long-distance and high-power communication systems. Consequently, numerous low SLL antenna arrays utilizing HWs have been investigated[22–29]. In[22], a nonequal waveguide power

[1]University of Kashan, School of Electrical and Computer Engineering, Kashan, Iran. [2]Graduate University of Advanced Technology, Electrical and Computer Department, Kerman, Iran. [3]Faculty of Electronics, Telecommunications, and Informatics, Gdańsk University of Technology, Department of Microwave and Antenna Engineering, 80–233, Gdańsk, Poland. ✉email: davood.zarifi@pg.edu.pl

divider was proposed to excite the radiation slots with a non-uniform amplitude distribution, resulting in an SLL of −25 dB over a frequency band from 14.15 to 16.25 GHz. However, this antenna array suffers from structure complexity and narrow bandwidth (13.8%). The design of a 2×2-element cavity-backed slot array with 13.4 dBi gain, 15% fractional bandwidth, −12dB SLL and 95% efficiency was reported in[24]. In[25], a low-sidelobe cavity-backed slot antenna array was proposed with 18.2 dBi gain, −20dB SLL, and 94% radiation efficiency. In[27], a 2×2-element cavity-backed slot array with 6.2% bandwidth, 97% total efficiency, 10.4–11 dBi realized gain and SLL of −14 dB was proposed. The design of a low-sidelobe 1×10-element slot array exhibited 13.1 dBi gain, −24.1dB SLL, and 1.8% fractional bandwidth[28]. The main drawback of that design is its ultra-narrow bandwidth.

To overcome the limitations of existing low SLL antenna arrays, this paper proposes a novel all-metal cavity-backed slot antenna array. The design directly excites each radiating slot through the cavity layer, eliminating the need for a complex power divider. The desired non-uniform amplitude distribution for SLL reduction is achieved by strategically positioning the radiating slots. Most of the cavity-backed slot arrays that use a single large cavity to excite the radiating slots exhibit narrow bandwidth. To overcome the bandwidth constraints typically associated with single-cavity designs, our proposed architecture incorporates two adjacent cavities with an integrated power divider. This configuration allowed us to achieve exceptional performance metrics, including a measured peak gain of 20.2 dBi and efficiency exceeding 90% across a 25% bandwidth spanning 3.1 to 4 GHz specifications that, to our knowledge, represent the first demonstration of such comprehensive performance in a fabricated low SLL cavity-backed antenna array. These features make the proposed antenna a promising candidate for sub-6 GHz networks requiring high gain, high efficiency, wide bandwidth, and low SLL.

The remainder of this paper is organized as follows: Sect. 2 explains the overall configuration of proposed antenna. The design methodology and simulated results of the proposed non-uniform excited cavity-backed slot array is presented in Sect. 3. Sections 4 and 5 discusses optimization process and the fabrication and measurement results, respectively. Finally, conclusions are provided in Sect. 6.

Antenna configuration

The configuration of the proposed antenna is illustrated in Fig. 1. The structure includes radiating elements in the top layer, two cavities in the middle layer, and a feeding network in the bottom layer, forming a three-layer metallic structure. This antenna features several key components: a 2-way coaxial-fed power divider, a cavity layer, 16 radiating slots arranged in a 4×4 array, and rectangular sidewalls employed as reflectors. The radiating slots are positioned on the top side of the cavity, while two coupling apertures are located on the bottom side. Input energy from the coaxial-to-waveguide transition is distributed to the coupling slots. Two matching steps at the waveguide ends facilitate a 2-way power division with minimal reflection loss across the 3–4 GHz operating band. The vertical sidewalls reduce off-axis radiation, minimizing sidelobes and improving overall performance. The frequency band of interest in the design is 3–4 GHz for various sub-6 GHz applications. The simulations and optimizations are performed by employing CST Microwave Studio.
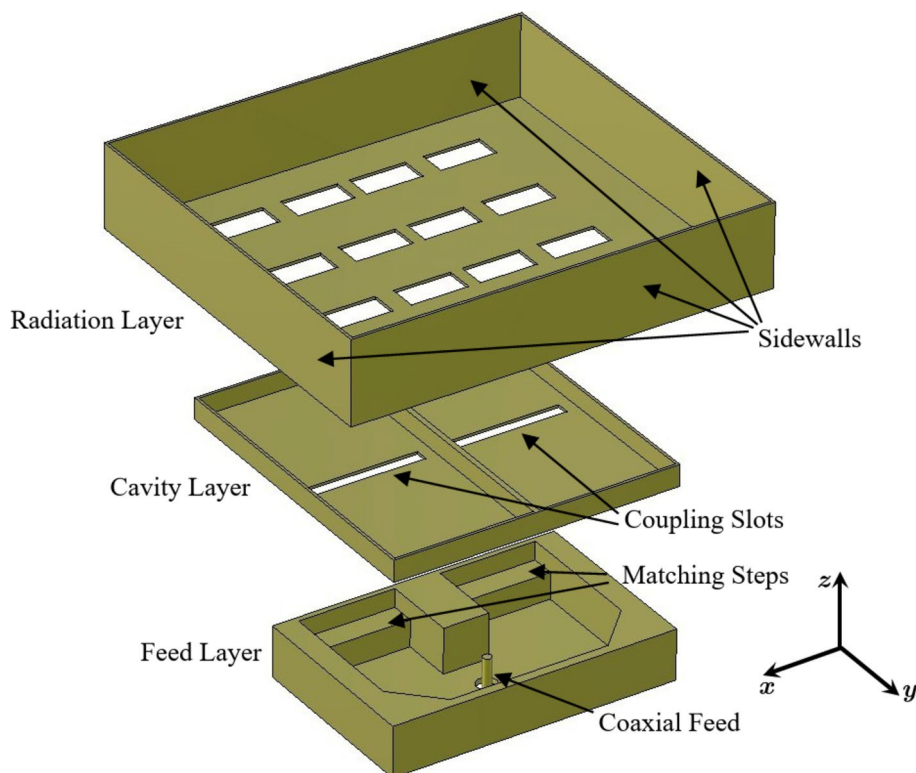

Fig. 1. Exploded perspective view of configuration of the proposed cavity-backed slot array antenna.

Antenna analysis and design
Array factor
The array factor (AF) for a planar 4×4-element array illustrated in Fig. 2(a) in the xy-plane is:

$$\mathrm{AF}(\theta, \varphi) = \sum_{n=1}^{4} \sum_{m=1}^{4} I_{mn} e^{j\alpha_{mn}} e^{j\psi_{mn}} \qquad (1)$$

where

$$\psi_{mn} = \beta \left(x'_{mn} \sin\theta \cos\varphi + y'_{mn} \sin\theta \sin\varphi \right) \qquad (2)$$

$$\alpha_{mn} = -\beta \left(x'_{mn} \sin\theta_0 \cos\varphi_0 + y'_{mn} \sin\theta_0 \sin\varphi_0 \right) \qquad (3)$$

where θ_0 and φ_0 define the main pointing direction, β is the phase constant of wave in free space, and I_{mn} and α_{mn} are the amplitude and phase of excitation. Given that all eight radiation elements are uniform in size, the critical factor for achieving the desired radiation performance is the spacing between the elements. Amplitude weighting, also called tapering, is a well-known technique used in array antenna design to reduce SLL. By adjusting the amplitude of the signals fed to each element in the array, the overall radiation pattern can be shaped to minimize sidelobes. Common amplitude weighting methods include using various distributions that gradually decrease the amplitude of the signals toward the edges of the array. This smooth tapering helps suppress sidelobes while maintaining the main lobe's integrity, thereby enhancing the antenna's signal-to-noise ratio and overall efficiency.

For this design, amplitude tapering along the y-axis is considered. This approach enables achieving the desired low SLL in the yz-plane. For instance, the AF corresponding to the in-phase excitation with amplitude coefficients of

$$\begin{bmatrix} 0.53 & 0.53 & 0.53 & 0.53 \\ 1 & 1 & 1 & 1 \\ 1 & 1 & 1 & 1 \\ 0.53 & 0.53 & 0.53 & 0.53 \end{bmatrix} \qquad (4)$$

for radiating elements and half-wavelength element spacing results in an SLL of -20 dB in the yz-plane of a broadside radiation pattern. The AF is calculated using (1)-(4) and illustrated in Fig. 2(b). To reduce the SLL in the xz-plane, we need to employ a different technique, which is discussed next.

Cavity-backed Radiation slots
As shown in Fig. 3(a) and (b), the radiation slots are initially identical and symmetrically arranged on the top surface of the cavity layer. This antenna features elements in a 4×4 configuration along the x- and y-axes. The slots are symmetrically positioned and exhibit symmetrical phase and amplitude excitation about the origin. The top side of the cavity features radiating slots, and the bottom side hosts two coupling apertures. The input energy from the feed layer is entered to the cavities through the coupling apertures for exciting the radiation slots. Taking into account the configuration of the radiating slots, it is evident that slots 1 and 2 have similar excitation characteristics. However, given that slot 2 is positioned further from the coupling slot, the amplitude of the excitation current is likely to be less than that of slot 4. This aspect of the current tapering can be utilized to reduce the side lobe level (SLL) in the yz-plane. The electric field distribution as shown in Fig. 4, indicates that the operational mode of cavities is TE_{150}, and its resonance frequency is given by:
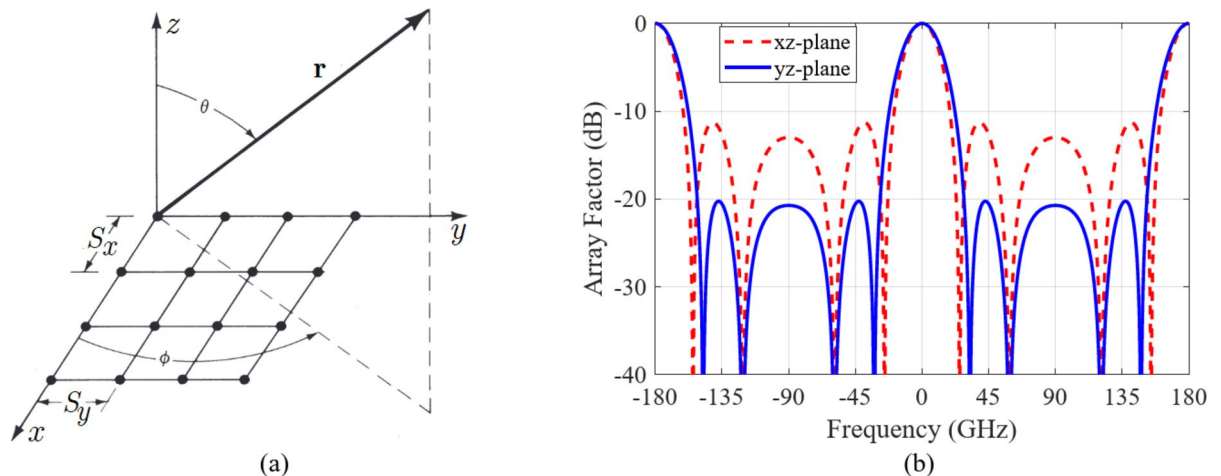

Fig. 2. (**a**) Geometry of 4×4-element planar antenna array. (**b**) Normalized AF in principal planes.
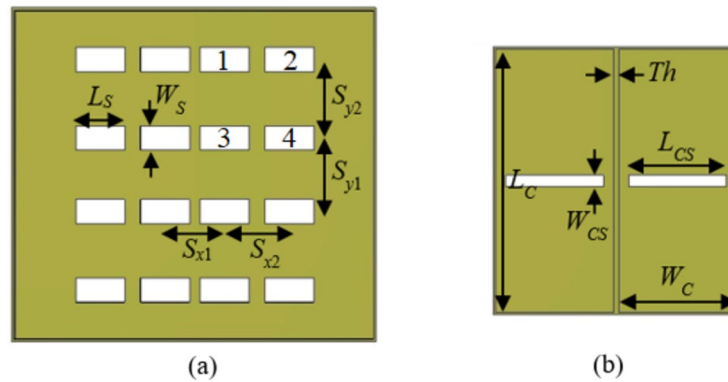
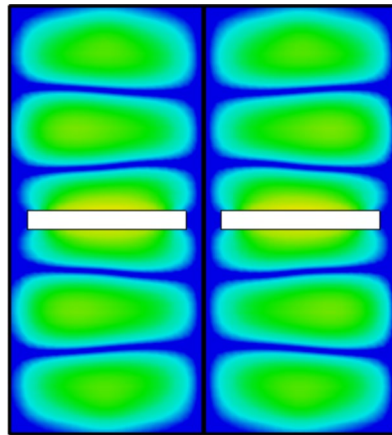Fig. 3. (a) Geometry of radiation slot array. (b) Configuration of cavity layer.

Fig. 4. Electric field distribution of cavity layer in 3.5 GHz.

$$f_r = \frac{1}{2\sqrt{\mu_o \varepsilon_0}} \sqrt{\left(\frac{1}{W_C}\right)^2 + \left(\frac{5}{L_C}\right)^2}. \tag{5}$$

Rectangular sidewalls as Reflector in Radiation Layer

As stated, by tapering the current amplitude of radiation elements along y-axis according to (5), the desired low SLL (−20 dB) in the yz-plane is achieved. Considering that the distribution of the excitation current of the radiating elements is assumed to be uniform along the x-axis, the SLL in the xz-plane is approximately −13 dB. To reduce this value, it is required to employ another technique. As illustrated in Fig. 5, four rectangular sidewalls with the same height and thickness are employed as a reflector for reducing undesirable radiations in side directions. The rectangular sidewalls help to minimize leakage current, which can cause diffraction at the edges of the metal plates surrounding the radiating slots. The idea is similar to employing a cylindrical shroud within a paraboloidal reflector enclosure to suppress the far-out sidelobes[30]. In addition, the height of the rectangular sidewalls must be optimized to achieve low SLL in the xz-plane. To demonstrate the impact of this parameter, the radiation patterns of the antenna with different rectangular sidewall heights are displayed in Fig. 6. The results indicate that the undesirable radiation of the antenna in the yz-plane is below −20 dB, attributed to the tapered amplitude of the element excitation currents. Consequently, adding rectangular sidewalls does not further enhance the SLL in this plane. However, using sidewalls with appropriate height reduces the SLL to approximately −20 dB in the xz-plane.

Feed Layer

A two-way power divide is required to ensure the cavity-backed slot array antenna is appropriately excitable. This power divider can be realized using a probe-fed rectangular waveguide junction. As depicted in Fig. 7, instead of using a conventional waveguide T-junction, a probe with a radius of R_P is placed exactly in the middle of two adjacent waveguides but not on the centerline of each of them. The impedance seen from the connector can be adjusted by changing this offset from the center O_P along with the length of the probe L_P As illustrated in Fig. 7, the waveguide has cross-sectional dimensions $W_W \times H_W$. The corners of waveguides are chamfered, and two stepped sections ($L_M \times W_M \times H_M$) are incorporated at the waveguide ends to facilitate the transformation
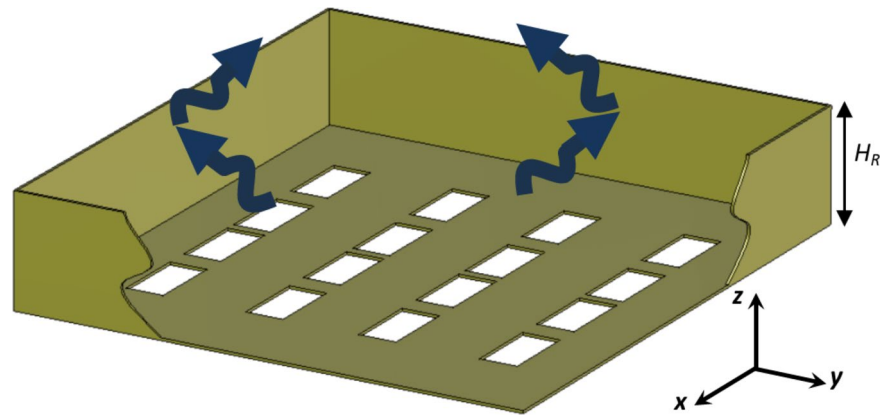
Fig. 5. Configuration of radiation slot array with rectangular sidewalls as reflectors.
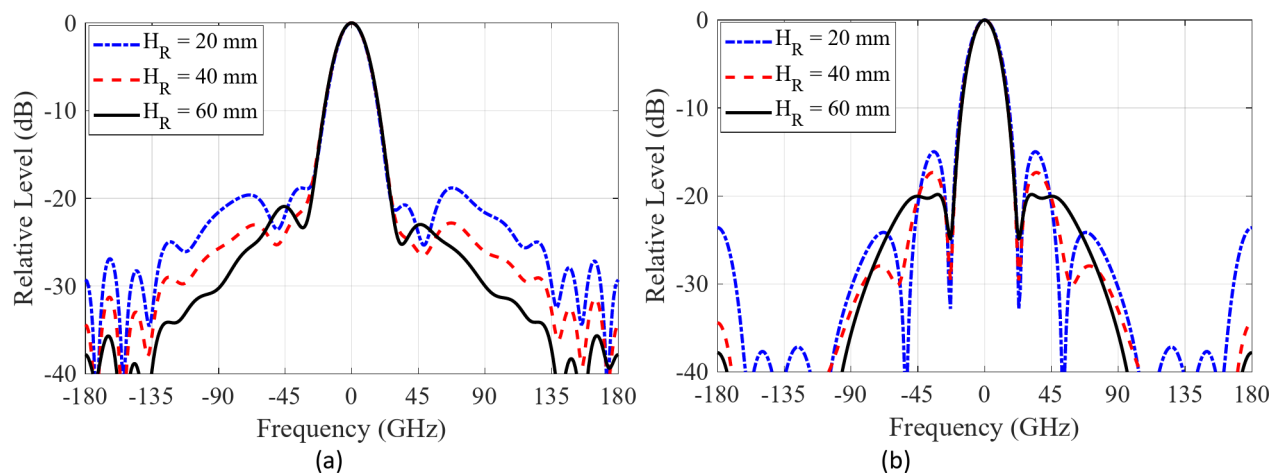

Fig. 6. Normalized radiation pattern of cavity-backed slot array with sidewalls with different heights. (**a**) yz-plane and (**b**) xz-plane.
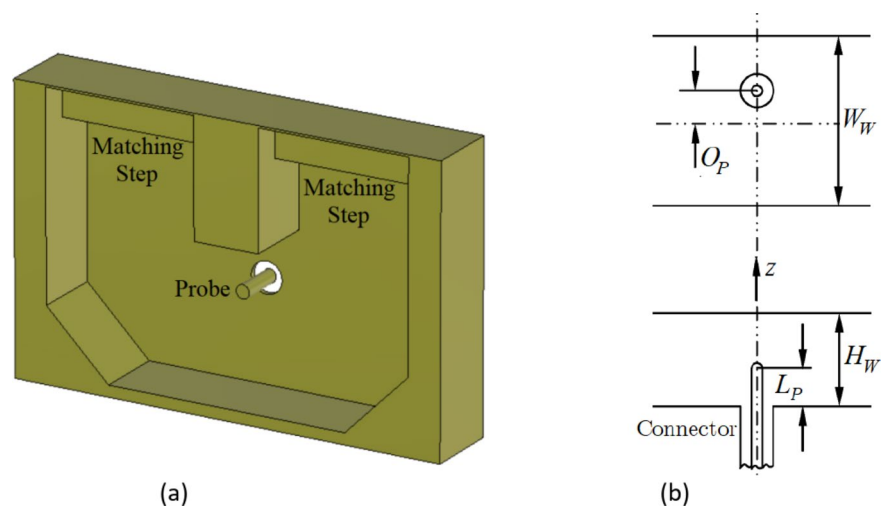

Fig. 7. (**a**) Geometry of probe-fed waveguide power divider. (**b**) Off-centerline probe-fed rectangular waveguide.
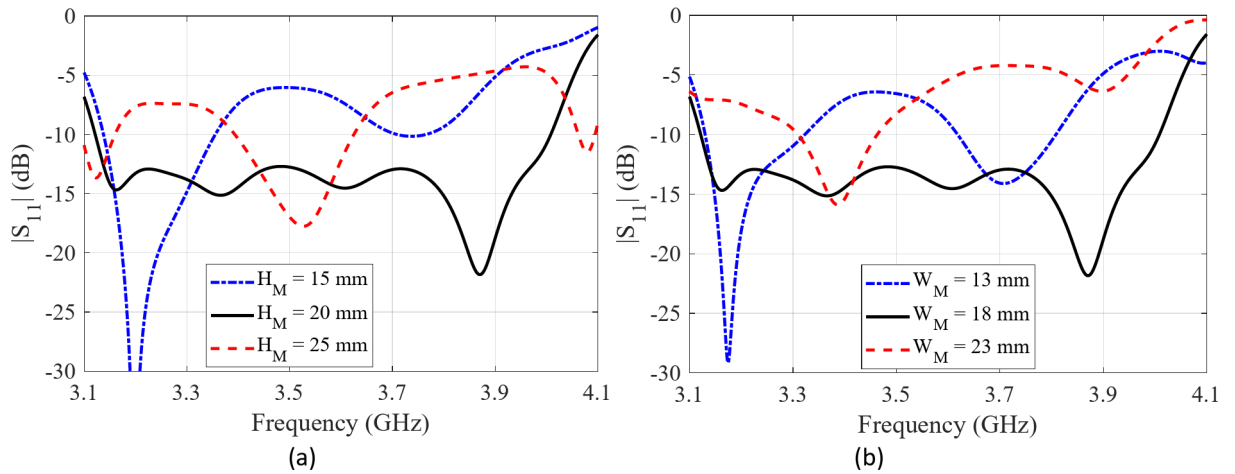
Fig. 8. Effect of height and width of matching steps the input reflection of the antenna.
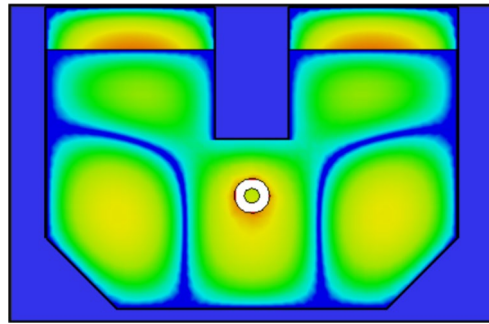

Fig. 9. Electric field distribution of power divider in 3.5 GHz.

of electromagnetic energy from the rectangular waveguides to the cavity layer via coupling slots, minimizing reflection loss.

The effect of height (H_M) and width (W_M) of matching steps on the performance of an antenna array was investigated by conducting several parameter studies (Fig. 8). It is evident that these geometrical parameters significantly impact the return loss at the input port of the antenna. The electric field distribution of the proposed power divider is displayed in Fig. 9.

Equivalent Circuit Model for feed layer

Detailed discussions on the classical setup of a rectangular waveguide to coaxial-line transition, with the probe located on the centerline of the waveguide's wide wall, can be found in the literature[31–34]. Since the electric current on the thin probe can be approximated by $I_0 \sin k_0(L_P\text{-}z)$, the input resistance can be determined as:

$$R_0 = \frac{Z_{TE_{10}}}{k_0^2 H_W W_W} \tan^2 \frac{k_0 L_P}{2} \qquad (6)$$

where $k_0 = \omega/c$ and Z_{TE10} is the impedance of TE_{10} mode in the rectangular waveguide given by:

$$Z_{TE_{10}} = \frac{120\pi}{\sqrt{1 - \left(\frac{\lambda}{2W_W}\right)^2}} \qquad (7)$$

A closed-form expression for the input resistance of an off-centerline probe can be obtained as follows: The fundamental mode's electric field in a rectangular waveguide is parallel to the probe axis, with its distribution across the waveguide axis described by $E_0 \cos(\pi O_P/W_W)$. In this equation, E_0 denotes the electric field intensity at the waveguide centerline. Consequently, the power delivered by a probe offset from the centerline by O_P is determined by the E-field's transverse position dependence, resulting in:

$$P = P_0 \cos^2 \left(\frac{\pi O_P}{W_W}\right) \qquad (8)$$

6

where P_0 represents the power delivered by the probe when it is positioned at the centerline of the waveguide's broad wall ($O_P = 0$). Consequently, the input resistance of a probe positioned off the centerline of the waveguide can be expressed as:

$$R_{in} = \frac{R_0}{\cos^2\left(\frac{\pi O_P}{W_W}\right)} = \frac{Z_{TE_{10}}}{k_0^2 H_W W_W}\tan^2\left(\frac{k_0 L_P}{2}\right)\left(1 + \tan^2\left(\frac{\pi O_P}{W_W}\right)\right) \tag{9}$$

An appropriate and simple equivalent circuit for the coaxial to rectangular waveguide junction aids conceptual design and enhances understanding of its functionality[33]. Figure 10 depicts a simple equivalent circuit of the junction. The probe passes through an aperture in the broad wall, modeled by an equivalent inductor (L_1) and capacitor (C_1). The proper equivalent circuit model for the probe in the waveguide includes a parallel combination of L_2 and C_2, which is connected in a shunt with the waveguide line. An ideal transformer is employed to scale the load impedances outside the waveguide environment. The scattering matrix corresponding to an ideal n:1 transformer is given by[35]:

$$[S] = \frac{1}{n^2 + 1}\begin{bmatrix} n^2 - 1 & 2n \\ 2n & 1 - n^2 \end{bmatrix} \tag{10}$$

Extracting the elements of the equivalent circuit yields $n = 1.29$, $L_1 = 46.41$ pH, $L_2 = 754.58$ pH, $C_1 = 4.63$ pF, and $C_2 = 2.01$ pF. The S-parameters for these extracted values are shown in Fig. 11, demonstrating a reasonable agreement with the CST full-wave simulation results.

Power Handling

The capacity of the proposed antenna to handle peak power relies on the dimensions of the structure. The maximum handled power P_{max} can be calculated as follows:

$$P_{\max} = \left(\frac{3 \times 10^6}{|E|_{\max}}\right)^2 \tag{11}$$

wherein represents the peak electric field value in the structure, calculated under the assumption of an input power of 1 W. As illustrated in Fig. 12, $|E|_{\max}$ at 3.5 GHz is 7226 V/m. Consequently, the antenna peak power handling capability is 172.3 kW.

Optimization process

The design process for the proposed cavity-backed slot array antenna, using a three-layer structure, involves these steps:

- Set the Design Frequency (f_0): Choose this frequency at the center of the desired bandwidth.
- Define Radiating Slot Dimensions ($L_S \times W_S$): Ensure these dimensions cause radiation over the target frequency range. Start with initial values of $\lambda_0/2 \times \lambda_0/4$ and set element spacing at $\lambda_0/2$.
- Specify Cavity Dimensions ($L_C \times W_C \times H_C$): Begin with initial dimensions of $\lambda_0 \times \lambda_0/2 \times \lambda_0/4$.
- Configure Waveguide Power Divider Dimensions: For a 1-to-2 rectangular waveguide-based power divider, start with width and height values of λ_0 and $\lambda_0/2$, respectively. Matching step dimensions can be initially λ_0 (length), $\lambda_0/4$ (width), and $\lambda_0/4$ (height).

- Determine Coaxial Line to Waveguide Transition: Begin with a probe length and offset of $\lambda_0/4$ and $\lambda_0/8$, respectively.
- Optimize the Design: Fine-tune 14 parameters, listed in Table 1., ensuring each parameter's allowable range is centered on its initial value, considering ±50% variations.

The optimization of the geometrical parameters of the proposed antenna geometry enables the attainment of the desired input reflection coefficient, gain, and SLL. This optimization is accomplished through the Trust
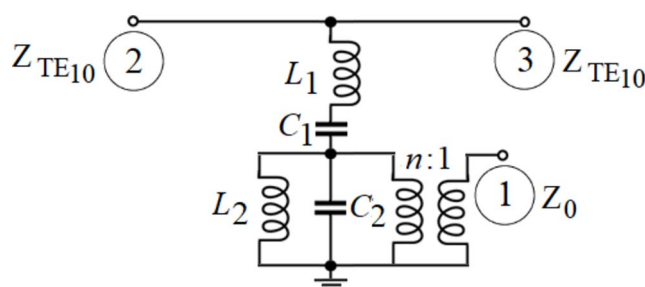
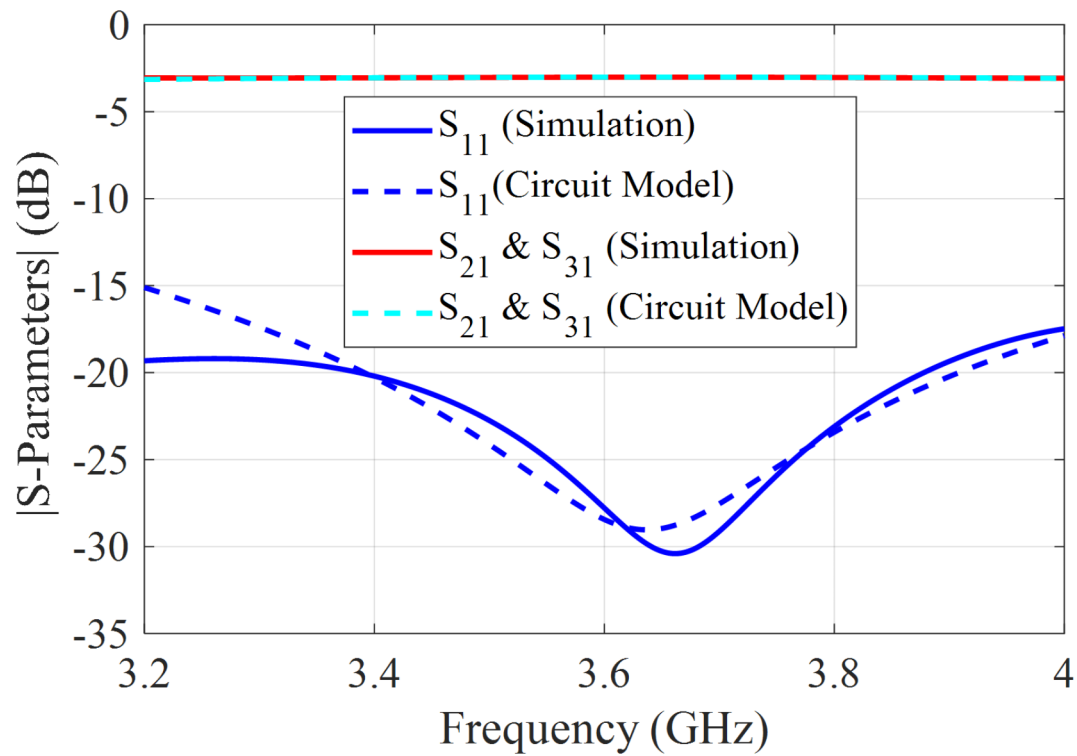**Fig. 10**. Equivalent circuit of coaxial-waveguide junction.

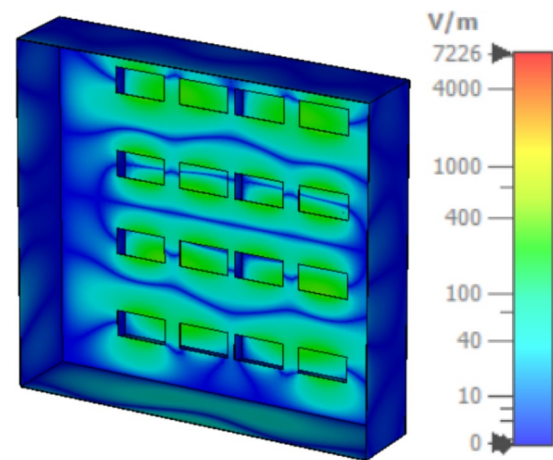**Fig. 11**. Comparison of *S*-parameters obtained with CST and the equivalent circuit model.

Fig. 12. Electric field distribution of cavity-backed slot array antenna in 3.5 GHz.

Parameter	L_S	W_S	S_{x1}	S_{x2}	S_{y1}	S_{y2}	W_{CS}	L_C	W_C
Value (mm)	42.07	20.72	47.74	55.36	62.78	68.87	9.93	221.84	103.1
Parameter	H_C	Th	L_M	W_M	H_M	O_P	L_P	W_W	H_W
Value (mm)	15.05	1	72.14	17.8	20.05	11.98	20.1	72.14	34.04

Table 1.. Optimized values for the geometrical parameters of the cavity-backed slot array.

Region Framework optimization method in CST Microwave Studio. The design specifications are met using CST's optimization tools with an appropriate fitness function defined as:
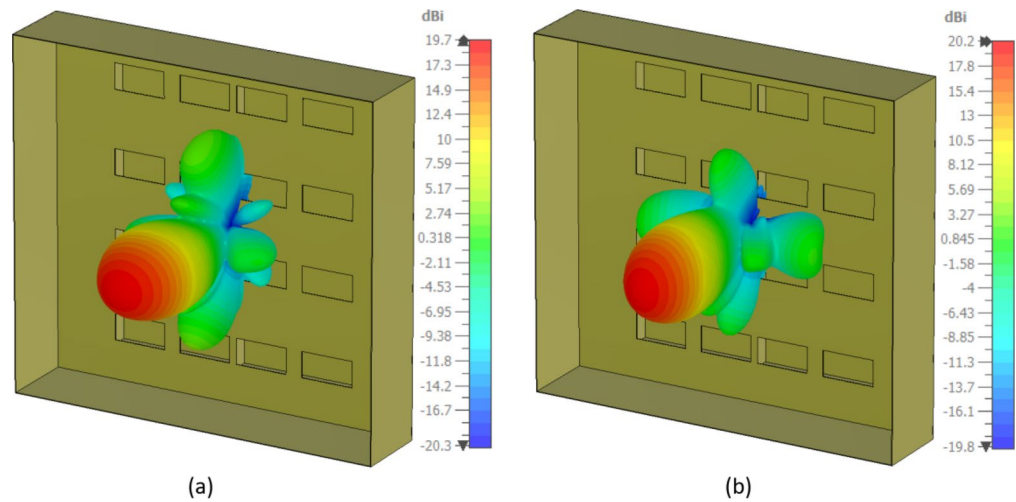
Fig. 13. 3-D radiation patterns of slot array antenna at (**a**) 3.3 and (**b**) 3.8 GHz.
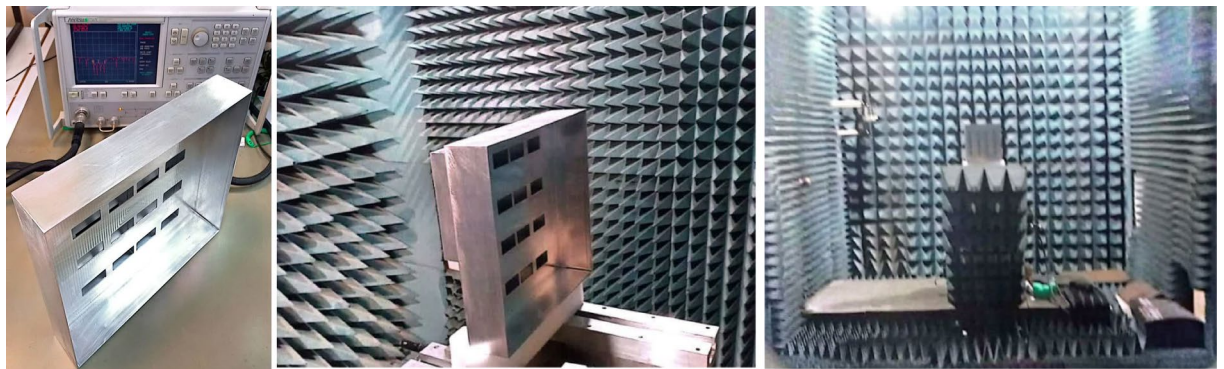

Fig. 14. The photographs of the fabricated antenna array under test.

$$fitness = \left(\frac{1}{M} \sum_{m=1}^{M} \left(|S_{11}(f_m)|^2 + |G(f_m) - G_0|^2 + |\text{SLL}(f_m) - \text{SLL}_0|^2 \right) \right)^{0.5} \tag{12}$$

where the input reflection coefficient and gain of the antenna at M frequency samples (f_m) over the required frequency band are represented by $S_{11}(f_m)$ and $G(f_m)$, respectively. The minimum realized gain and SLL are selected as $G_0 = 20$ dBi and $\text{SLL}_0 = -20$ dB for the optimization procedure. On a Windows 10 system with an Intel Xeon Gold 6136 CPU (3.5 GHz, two processors, 36 cores) and 576 GB of RAM, the optimization process takes less than one minute per full structure simulation.

The values of the final optimized parameter are detailed in Table 1.. The 3-D radiation patterns of the optimized antenna at 3.3 and 3.8 GHz are displayed in Fig. 13. Observe that the simulated realized gain is approximately 20 dBi over the desired frequency bandwidth.

Fabrication, measurement and discussion
Measurement results
The concept was illustrated by fabricating a prototype of the cavity-backed slot array antenna using aluminum. Figure 14 presents the fabricated prototype under test. The standard N-type connectors used have a probe diameter of 3 mm. S_{11} measurement of the prototype is conducted using an Anritsu 37,347 C network analyzer. Figure 15 compares the simulated and measured S- parameters, revealing that the measured $|S_{11}| < -10$ dB bandwidth ranges from 3.1 to 4 GHz. The slight discrepancy between the measurement and simulation values can be caused by fabrication tolerance.

The far-field radiation pattern and gain are measured in an anechoic chamber with a resolution of 1° rotation. The normalized simulated and measured radiation patterns of the antenna array are shown in Fig. 16. Consistent with the simulation responses, the measured radiation pattern exhibits no beam squint. The measured peak gain of the antenna is approximately 20.2 dBi, compared to the simulated gain of 20.7 dBi, with a reduced SLL of −19 dB. The measured results align well with the simulations, validating the design. Minor deviations between the
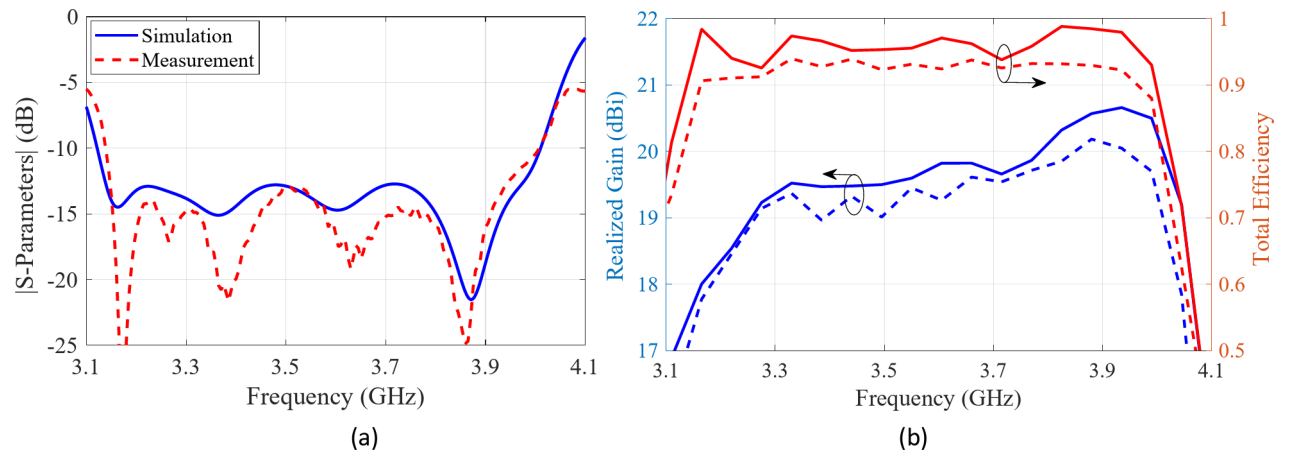
Fig. 15. Simulated and measured (**a**) input reflection coefficient and (**b**) realized gain and total efficiency of cavity-backed slot array antenna.
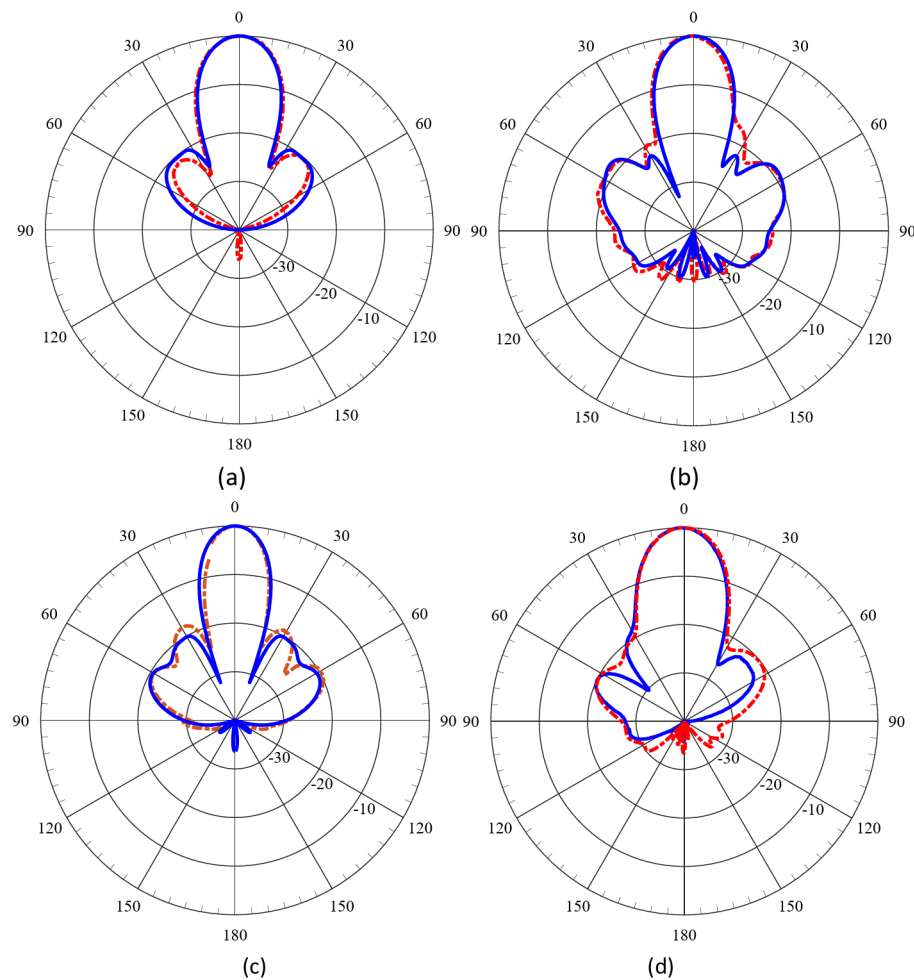

Fig. 16. Simulated (solid lines) and measured (dashed-lines) normalized radiation patterns of antenna array in E- and H-planes at 3.3 GHz (**a** and **b**) and 3.8 GHz (**c** and **d**).

Ref	Technology	Size of Array	f_0 (GHz)	Bandwidth (%)	Gain (dBi)	SLL (dB)	Efficiency (%)
[14]	PCB	1×3	13.2	3.4	11.6	−19	85
[20]	PCB	6×16	10	7.15	21.92	−29.1	NA
[23]	HW	4×4	10	10	20.3	−12	NA
[24]	HW	2×2	4	15	13.4	−13	98
[25]	HW	5×4	3.43	0.5	18.2	−20	94
[27]	HW	2×2	3.71	6.2	11	−14	97
[28]	HW	1×10	4.92	1.8	13.1	−24.1	82
[29]	HW	5×6	10	1	18.4	−13	90
This Work	HW	4×4	3.55	25.3	20.2	−19	80–94

Table 2. Performance comparison of the cavity-backed antenna arrays.

measured and simulated results may be attributed to fabrication tolerances and inaccuracies in the measurement setup.

Discussion

Table 2 compares the performances of previously reported cavity-backed array antennas with the proposed design. With a fractional bandwidth of 25.3% from 3.1 GHz to 4 GHz, our three-layer structure surpasses the limited bandwidth of most single-cavity-backed slot arrays. By employing a cavity layer with two adjacent rectangular cavities and an appropriate power divider, our antenna achieves the broadest impedance bandwidth among similar designs while maintaining low SLL, high gain, and acceptable total efficiency. These characteristics render it highly suitable for sub-6 GHz communications.

Conclusion

This study presents the design and implementation of an all-metal wideband slot array antenna tailored for 5G sub-6 GHz networks. The comprehensive validation through simulations and experimental measurements confirms the antenna's capability for wideband operation with high gain, low reflection loss, and high efficiency over the frequency band from 3.1 to 4 GHz. Overall, the proposed low SLL wideband antenna is crucial for enhancing signal clarity and mitigating interference, which are essential for 5G and next-generation wireless communications.

Data availability

All data generated or analyzed during this study are included in this published article.

References

1. Rappaport, T. S. et al. Millimeter wave mobile communications for 5G cellular: it will work! *IEEE Access.* **1**, 335–349 (2013).
2. Hong, W. et al. Jan., The Role of Millimeter-Wave Technologies in 5G/6G Wireless Communications, *IEEE Journal of Microwaves*, vol. 1, no. 1, pp. 101–122, (2021).
3. Huang, G., Zhou, S., Chio, T., Hui, H. & Yeo, T. A low profile and low sidelobe wideband slot antenna array fed by an amplitude-tapering waveguide feed-network. *IEEE Trans. Antennas Propag.* **63** (1), 419–423 (Jan. 2015).
4. Guo, J., Hu, Y. & Hong, W. A 45° polarized wideband and wide-Coverage Patch antenna array for millimeter-Wave communication. *IEEE Trans. Antennas Propag.*, **70**, 3, pp. 1919–1930, March 2022.
5. Tomura, T., Hirokawa, J., Hirano, T. & Ando, M. A 45° linearly polarized hollow-waveguide 16×16-slot array antenna covering 71–86 GHz band, *IEEE Trans. Antennas Propag.*, vol. 62, no. 10, pp. 5061–5067, Oct. (2014).
6. You, Y. et al. Oct., High-performance E-band continuous transverse stub array antenna with a 45° linear polarizer, *IEEE Antennas Wireless Propag. Lett.*, vol. 18, no. 10, pp. 2189–2193, (2019).
7. Zhang, L. et al. Wideband 45° linearly polarized slot array antenna based on gap Waveguide Technology for 5G millimeter-Wave Applications. *IEEE Antennas. Wirel. Propag. Lett.* **20** (7), 1259–1263 (July 2021).
8. Varum, T., Matos, J. N., Pinho, P. & Abreu, R. Nonuniform broadband circularly polarized antenna array for vehicular communications, *IEEE Trans. Veh. Technol.*, vol. 65, no. 9, pp. 7219–7226, Sep. (2016).
9. Chen, F. C., Hu, H. T., Li, R. S., Chu, Q. X. & Lancaster, M. J. Design of filtering microstrip antenna array with reduced sidelobe level. *IEEE Trans. Antennas Propag.* **65** (2), 903–908 (Feb. 2017).
10. Boskovic, N., Jokanovic, B. & Radovanovic, M. Printed frequency scanning antenna arrays with enhanced frequency sensitivity and sidelobe suppression, *IEEE Trans. Antennas Propag.*, vol. 65, no. 4, pp. 1757–1764, Apr. (2017).
11. Ogurtsov, S. & Koziel, S. On alternative approaches to design of corporate feeds for low-sidelobe microstrip linear arrays, *IEEE Trans. Antennas Propag.*, vol. 66, no. 7, pp. 3781–3786, Jul. (2018).
12. Mardani, H., Nourinia, J., Ghobadi, C., Majidzadeh, M. & Mohammadi, B. A compact low-side lobes three-layer array antenna for X-band applications. *AEU-Int J. Electron. Commun.* **99**, 1–7 (Feb. 2019).
13. Kalva, N. & Kumar, B. M. Feedline Design for a Series-Fed Binomial Microstrip antenna array with no sidelobes. *IEEE Antennas. Wirel. Propag. Lett.* **22** (3), 650–654 (March 2023).
14. Yan, Y. X., Huang, Y. X., Tang, S. C. & Chen, J. X. Low-Sidelobe Microstrip Patch Filtenna Array Fed by Higher Order Mode SIW Cavity, *IEEE Antennas and Wireless Propagation Letters*, vol. 22, no. 8, pp. 1873–1877, Aug. (2023).
15. Chandan, R. K. & Pal, S. Low SLL enhanced gain proximity coupled linear antenna array for 5G wireless communications, *AEU-Int. J. Electron. Commun.*, vol. 175, Feb. (2024).

16. Yang, H. et al. Improved Design of low sidelobe substrate Integrated Waveguide Longitudinal slot array. *IEEE Antennas. Wirel. Propag. Lett.* **14**, 237–240 (2015).
17. Park, S. J., Shin, D. H. & Park, S. O. Low side-lobe substrate integrated waveguide antenna array using broadband unequal feeding network for millimeter-wave handset device. *IEEE Trans. Antennas Propag.* **64** (3), 923–932 (Mar. 2016).
18. Cheng, Y. J., Wang, J. & Liu, X. L. 94 GHz substrate integrated waveguide dual-circular-polarization shared-aperture parallel-plate long-slot array antenna with low sidelobe level, *IEEE Trans. Antennas Propag.*, vol. 65, no. 11, pp. 5855–5861, Nov. (2017).
19. Lin, W. & Ziolkowski, R. W. Compact, Highly Efficient Huygens Antenna Array with Low Sidelobe and Backlobe Levels, *IEEE Transactions on Antennas and Propagation*, vol. 69, no. 10, pp. 6401–6409, Oct. (2021).
20. Trinh, T. V., Trinh-Van, S., Lee, K. Y., Yang, Y. & Hwang, K. C. Design of a low-cost low-sidelobe-level differential-fed SIW slot array antenna with zero beam squint. *Appl. Sci.* **12** (21), 10826 (Oct. 2022).
21. Wang, S., Zhou, B. & Fang, G. A method for low Sidelobe substrate-integrated Waveguide Slot Antenna Design Applied for Millimeter-Wave radars. *Remote Sens.*, **16**, 3, pp.474, (2024).
22. Huang, G. L., Zhou, S. G., Chio, T. H., Hui, H. T. & Yeo, T. S. A low Profile and low sidelobe wideband slot antenna array Feb by an amplitude-tapering Waveguide feed-Network. *IEEE Trans. Antennas Propag.* **63** (1), 419–423 (Jan. 2015).
23. Mahmud, Y. R. H. & Lancaster, M. J. High-gain and wide-bandwidth filtering planar antenna array-based solely on resonators. *IEEE Trans. Antennas Propag.* **65** (5), 2367–2375 (May 2017).
24. Chen, R. S. et al. Aug., High-Efficiency and Wideband Dual-Resonance Full-Metal Cavity-Backed Slot Antenna Array, *IEEE Antennas and Wireless Propagation Letters*, vol. 19, no. 8, pp. 1360–1364, (2020).
25. Chen, R. S. et al. Low-sidelobe cavity-backed slot antenna array with simplified feeding structure for Vehicular communications. *IEEE Trans. Veh. Technol.* **70** (4), 3652–3660 (April 2021).
26. Chen, R. S. et al. Sept., S-band full-metal circularly polarized cavity-backed slot antenna with wide bandwidth and wide beamwidth, in *IEEE Transactions on Antennas and Propagation*, vol. 69, no. 9, pp. 5963–5968, (2021).
27. Chen, R. S., Wong, S. W., Huang, G. L., He, Y. & Zhu, L. Bandwidth-Enhanced High-Gain Full-Metal Filtering Slot Antenna Array Using TE101 and TE301 Cavity Modes, *IEEE Antennas and Wireless Propagation Letters*, vol. 20, no. 10, pp. 1943–1947, Oct. (2021).
28. Li, H. & Li, Y. Low-Sidelobe Antenna Array Based on Evanescent Mode of Cutoff Waveguide, *IEEE Transactions on Antennas and Propagation*, vol. 70, no. 12, pp. 11608–11616, Dec. (2022).
29. Lin, J. Y., Yang, Y., Wong, S. W. & Chen, R. S. In-Band full-duplex filtering antenna arrays using High-Order Mode Cavity resonators. *IEEE Trans. Microwave Theory Tech.* **71** (4), 1630–1639 (April 2023).
30. Narasimhan, M., Raghavan, K. & Ramanujam, P. GTD analysis of the radiation patterns of a prime focus paraboloid with shroud. in *IEEE Trans. Antennas Propag.*, **31**, 5, pp. 792–794, September 1983.
31. Bialkowski, M. E. & Khan, P. J. Determination of the admittance of a general waveguide-coaxial line junction, *IEEE Trans. Microw. Theory Tech.*, vol. MTT-32, no. 4, pp. 465–467, Apr. (1984).
32. Collin, R. E. Foundations for Microwave Engineering, Hoboken, NJ, USA:Wiley, (2007).
33. Yeap, K. H., Tham, C. Y., Nisar, H. & Loh, S. H. Analysis of probes in a rectangular waveguide, *Frequenz*, vol. 67, no. 5, pp. 145–154, Jan. (2013).
34. Eshrah, I. A., Kishk, A. A., Yakovlev, A. B., Glisson, A. W. & Smith, C. E. Analysis of waveguide slot-based structures using wide-band equivalent-circuit model, *IEEE Transactions on Microwave Theory and Techniques*, vol. 52, no. 12, pp. 2691–2696, Dec. (2004).
35. Ludwig, R. & Bogdanov, G. *RF Circuit Design: Theory and Applications*, London, U.K.:Pearson, (2010).

Acknowledgements

Author contributions

D. Z. contributed to the conceptualization and design of the study and was involved in the drafting of the manuscript. A. F. contributed to the conceptualization and design of the study and was involved in the drafting of the manuscript. M. M. supervised the design and was involved in the drafting of the manuscript.

Declarations

Competing interests

The authors declare no competing interests.

Additional information

Correspondence and requests for materials should be addressed to D.Z.

Reprints and permissions information is available at www.nature.com/reprints.

Publisher's note Springer Nature remains neutral with regard to jurisdictional claims in published maps and institutional affiliations.